


Time-Resolved Magneto-Optical Investigations of Picosecond Magnetisation Dynamics in Arrays of Non- Ellipsoidal Ferromagnetic Nano-Elements

Submitted by **Paul Steven Keatley**, to the University of Exeter
as a thesis for the degree of Doctor of Philosophy in Physics,
June 2008.

This thesis is available for Library use on the understanding that it is copyright material and that no quotation from the thesis may be published without proper acknowledgement.

I certify that all material in this thesis which is not my own work has been identified and that no material has previously been submitted and approved for the award of a degree by this or any other University.

A handwritten signature in black ink, appearing to read 'P. Keatley', written over a horizontal dotted line.

Abstract

In this thesis the results of magneto-optical experiments will be presented. The experiments were performed on micro-arrays of square nanomagnets in order to characterise the static and time-dependent behaviour of the nanomagnets. The static behaviour was investigated in vector-resolved scanning Kerr microscopy experiments, while the time-dependent behaviour was investigated in time-resolved scanning Kerr microscopy experiments. In the latter so-called pump-probe experiments, magnetisation dynamics were induced by exciting the sample magnetisation with a pulsed magnetic field (pump). The magnetisation dynamics were then detected using the magneto-optical polar Kerr effect (probe). The longitudinal Kerr effect was utilised in the vector-resolved scanning Kerr microscope in order to measure the in-plane components of the static magnetisation. The experimental set-up and methodology of the vector- and time-resolved scanning Kerr microscopy experiments will be discussed in detail, in particular, the detection technique that allows three components of the vector magnetisation to be measured simultaneously. Since the spatial resolution of the magneto-optical probe was insufficient to resolve the spatial character of the magnetisation dynamics within individual nanomagnets, micromagnetic simulations were used to gain insight into the character of the excited modes. Extensive testing of different micromagnetic models was carried out in order to investigate the effect of the different models on the simulated dynamics. The results of measurements carried out on the arrays of square nanomagnets revealed that the static and time-dependent behaviour of the magnetisation became more complicated as the size of the nanomagnets was reduced. In particular, similar hysteresis loops were acquired when the elements were magnetised along the uniaxial anisotropy easy and hard axes, while fast Fourier transform spectra of time-resolved signals revealed that the character of the magnetisation dynamics changed significantly as the element size and/or applied magnetic field were reduced. Interpretation of the experimental results using micromagnetic simulations revealed that the elements had a non-uniform single domain ground state magnetisation. When the field was applied along either edge of the square elements and reversed, the magnetisation was found to switch via a series of metastable non-uniform single domain states. Furthermore, the increasing non-uniformity of the single domain ground state as the element size and/or applied field were reduced lead to significant changes in the mode character excited within the elements. Comparison of

experimental spectra with simulated spectra and Fourier images of the dynamic magnetisation revealed that as the element size and/or applied field were reduced, the mode character changed from one that occupied the majority of the volume of the element, to several modes that were localised near to the edges of the element that were perpendicular to the applied field. Furthermore, deviation of the direction of the wavevector of the dynamic magnetisation from the direction of the static magnetisation was found to lead to a dynamic configurational anisotropy within nanomagnets. Following the presentation of the experimental results, the recent developments for future experimental work are presented with the aim to study precessional switching in an isolated nanomagnet. The results obtained in the experiments presented in this thesis are expected to lead to a better understanding of the non-uniform magnetisation dynamics in square nanomagnets, which have application in future magnetic data storage technologies.

To My Parents

Acknowledgements

The work presented in this thesis, and indeed this thesis itself, represents the cumulative help and support of my colleagues, friends, and family. This part of the thesis has proved to be more difficult to write than any other section in this thesis. The people that I've had the pleasure of spending time with at school, in the Air Training Corps, at sixth form, in part-time jobs, and as an undergraduate and postgraduate student, have all influenced me in one way or another. The innumerable influences, the smallest comment, compliment or criticism, have ultimately motivated me to complete my PhD and write this thesis. While it is impossible to acknowledge all of those people here, I will always remember them, and hopefully they will know their contribution to this work by making me the person I am today.

I would like to acknowledge the influence of several people in particular. To begin with I would like to thank my PhD supervisor, Prof Rob Hicken, for accommodating me on this research project at such short notice. I will always be grateful to Rob for his unwavering dedication, encouragement, and advice throughout. I would also like thank Rob for providing the opportunity to work on experiments at synchrotron facilities, and to present my work to wider audiences at several international conferences, both of which have been invaluable experiences for me. Finally, I would like to thank Rob for his time to read and critically comment on several versions of this thesis. Thank you Rob.

Past and present members of the Magnetic Materials Group have made it a stimulating group to work in. Thanks to Dr Anjan Barman and Dr Volodymyr Kruglyak for teaching me how to perform time-resolved magneto-optical microscopy experiments. A separate thanks to Volodymyr for his advice on anything physics (and more) each time I came knocking on his office door, which was pretty much a daily event. Thanks to Dr Ralph Wilks for his advice on magneto-optics and the use of electronics for the detection magneto-optical effects. Thanks to Dr Sam Ladak for helping me to settle in very quickly, and for providing the magnetic film used in experiments that led to my first paper. Thanks to Mr Shemaiah Weekes for being a superb comrade to whom I could grumble when my experiments were less than successful, and for driving for the entire time on our road trip across California. Thanks to Mr Leigh Shelford and Dr Yanwei Liu for allowing me to exercise my teaching skills by demonstrating magnetometry experiments when they first joined the group. Thanks

to Dr Andreas Neudert for bringing fresh ideas to the time-resolved experiments in Exeter, and for numerous discussions on theoretical magnetism and magneto-optics whilst I was writing this thesis. Thanks to Dr Feodor Ogrin for the opportunity to work on some of his experiments at synchrotron facilities, and for introducing me to Russian humour. Last and certainly not least, thanks to Mr Russell Edge for the excellent quality of the equipment that you created from nothing more than my scrappy sketches. The experiments presented in this thesis could not have been performed without first-rate equipment, advice and encouragement. Thank you all.

I would like to thank Prof Peter Winlove for agreeing to be my PhD mentor and internal examiner. Peter was my second year undergraduate tutor and has always kept an open door for me. I have very much enjoyed my mentor meetings with Peter during my PhD. These meetings allowed me to reflect on my work and appreciate that I was making good and steady progress throughout my PhD, which is sometimes difficult to see when your in the thick of it. Thank you Peter.

In addition to the people already mentioned, friends and colleagues outside of the Magnetic Materials Group have also made my time as a PhD student a rich and memorable one. Thanks to Dr Nathan Mayne, Dr Luke Hounsome, Dr Matthew Eames, Dr Steven Paul Hepplestone, and Dr Gemma Winter who have all been here from the outset in 1999. It's been a long slog, which seemed longer for me since most of you guys got your PhDs a whole graduation year before me. Thanks to Nathan for being there to talk sense into me when anything was getting me down, and for letting me win "The Epic" game of squash in our fourth year as undergraduates. Thanks to Luke and his wife Catherine for a great three years at 11 Old Park Road, and for inviting me to be Luke's Best Man at their wedding. I realised that I was definitely The Best Man when I caught the largest (12 lb) Pollock on the stag weekend. I would also like to thank Dr Steve Sque, Dr Eric Saunders and Dr Neil Telling for helpful advice whilst I was writing this thesis. A separate thanks to Neil for introducing me to synchrotron experiments and broadening my experimental expertise. Thanks to Dr Andrew Murray for acquiring high resolution scanning electron microscope images of the samples at short notice for the post viva corrections to this thesis. Thanks to Dr Ian Hooper and Dr Peter Vukusic for their support on the wicket despite my poor batting ability outside the nets. Thanks to Dr Matthew Lockyear for kind-of-helpful advice while writing this thesis, "Just get it done, son". Finally, separate thanks to Nathan, Leigh, Matt Eames, Steve Hepplestone, Andreas, and Volodymyr for reading and critically commenting on various chapters and sections of this thesis.

Next I would like to thank the brilliant support staff in the School of Physics for their help during my PhD. Firstly, thanks to Mr Kevyn White, Mr David Jarvis, Mr John Meakin, Mr Peter Cann and the other guys in the ground floor workshops. Thanks to Kev for the excellent quality of the optical detectors that he constructed for the experiments, and to Dave for evaporating anti-reflective coatings onto some of the samples. Thanks to John for his array of odds and ends tucked away in Stores that became necessary parts for many experiments. A separate thanks to Kev, John, and Pete for cheerleading duties at the occasional Nomads cricket match. Thanks to Mr Chris Forrest for helping to solve PC problems at short notice, and to Dr Charles Williams and Mr Tom Addison for helpful advice while I was re-designing and building the electronics for the optical detectors. Finally I would like to thank the administrative staff, in particular Mrs Natalia Ogrina, Mrs Denise Watts and Mrs Hilary Jordan, for figuring out all of my claim and order forms, which I'm just about getting the hang of. A separate thanks to Mrs Valerie Barnes, Mrs Lynda Barrell, and Mrs Victoria Brown for making sure I always had enough to eat after school open days.

Outside of the School of Physics I have an fantastic network of friends who have always encouraged and supported me. Many of my closest friendships in Exeter were made during the three years that I worked at the Imperial during my undergraduate degree. In particular, thanks to Jane and Dolly (Mr and Mrs Knott) and to Dr Lizzie Thompson for listening to me ramble on about magnets and lasers, and for always being there when anything was getting me down. I will always be grateful to Jane for introducing me to music festivals, which I adopted as an annual break from my PhD research. And thanks to Dolly for his faith. Dolly has been calling me Doctor since I started my PhD, therefore I'm glad I was successful as I think the nickname has now stuck. Thank you all for an outstanding five or six years, they seem to have gone far too quickly, but it was a great laugh.

It wasn't until I started my Physics A-Level that I began to find Physics really stimulating. Therefore, I would like to thank my excellent Physics A-level teachers at Newquay Treviglas School, Dr Jeremy Pollard and Mrs Jane Willmott, for making Physics an exciting subject to study, and for encouraging me to study Physics at University. I think it's fair to say that Dr Pollard, a former undergraduate and postgraduate student in the School of Physics at Exeter, nudged me in the direction of Exeter for which I will always be grateful.

My family have been a huge inspiration. I would like to thank my parents Sonia and Peter, and my younger sister Steph. My parents have led by example and shown my sister and I that fantastic achievements are the result of hard work and dedication, and that there are no easy routes. All Mum and Dad have ever asked of me (excluding chores and being nice to my sister) is that I do my best, and they would support me whatever I chose to do. I cannot thank you both enough for all of your love and support over the last twenty-seven years. I can honestly say that I did my best. Not bad for a “small child”. Thank you Mum, Dad and Steph.

Finally I would like to thank my partner Kelly. Not only did Kelly buy me drum lessons to take my mind off this thesis for one hour every other week, but Kelly has offered endless support, encouragement and love over the last year whilst I was writing this thesis. It's been a tough year, but we made it together. I can now play my drums guilt-free in the knowledge that this thesis is complete, and we can now have that skiing holiday. Thank you Kelly, I love you lots.

List of Contents

Title Page	1
Abstract	2
Acknowledgements	4
List of Contents	9
List of Publications	11
List of Figures	13
List of Tables	24
Declaration	25
Chapter 1 <i>Introduction</i>	28
Chapter 2 <i>Background concepts of magnetism</i>	34
2.1 Introduction	34
2.2 Classification of magnetic materials	34
2.3 Diamagnetism.....	35
2.4 Permanent atomic moments	37
2.5 Paramagnetism	41
2.6 Ferromagnetism.....	43
2.7 The exchange interaction.....	48
2.8 Band model theories of ferromagnetism	55
2.9 Ferromagnetic free energy contributions	57
2.10 The magnetisation of a ferromagnetic material.....	66
2.11 The Stoner-Wohlfarth model.....	72
2.12 Ferromagnetic resonance.....	76
2.13 The magnetic equation of motion.....	77
2.14 The Kittel formula	79
2.15 Magnetostatic spin wave modes.....	82
2.16 Spin wave modes in thin films	84
2.17 Spin waves in small non-ellipsoidal elements.....	85
2.18 Summary	89
Chapter 3 <i>Experimental techniques</i>	90
3.1 Introduction	90
3.2 Magneto-optical effects in metals	90
3.3 The magneto-optical reflection coefficients.....	96
3.4 The magneto-optical Kerr effect geometries.....	99
3.5 Detection of the magneto-optical Kerr effect.....	101
3.6 Time resolved scanning Kerr microscopy.....	109
3.7 Experimental limitations and modifications.....	121
3.8 Summary	126
Chapter 4 <i>Acquisition of vector hysteresis loops from microarrays of nanomagnets</i>	127
4.1 Introduction	127
4.2 Experimental and sample details.....	128

4.3 Results and discussion.....	139
4.4 Summary	148
Chapter 5 Use of microscale coplanar stripline with indium tin oxide windows in optical ferromagnetic resonance measurements	149
5.1 Introduction	149
5.2 Sample and experimental details	150
5.3 Results and discussion.....	153
5.4 Summary	157
Chapter 6 Time-resolved investigation of magnetisation dynamics of arrays of non-ellipsoidal nanomagnets with a non-uniform ground state	158
6.1 Introduction	158
6.2 Sample and experimental details	161
6.3 Details of numerical simulations	164
6.4 Results and discussion.....	169
6.5 Collective modes within arrays	192
6.6 Summary	194
Chapter 7 Dynamic configurational anisotropy in nanomagnets	196
7.1 Introduction	196
7.2 Sample and experimental details	198
7.3 Experimental and numerical results	200
7.4 Discussion	206
7.5 Summary	208
Chapter 8 Recent developments for future work.....	209
8.1 Introduction	209
8.2 Recent developments.....	210
8.3 Experimental set-up.....	210
8.4 Antireflective coatings	221
8.5 Vector- and time-resolved scanning Kerr microscopy	225
8.6 Summary	231
Chapter 9 Summary	232
Appendix 1 Calculation of the vector bridge longitudinal Kerr signal for the component of magnetisation perpendicular to the applied field	236
Appendix 2 Time-resolved scans acquired from arrays of nanomagnets	238
Appendix 3 The probe station assembly	240
Appendix 4 Tuning of the servomechanism loop gain	243
Appendix 5 The Mk II vector bridge detector	244
Bibliography	246

List of Publications

1. P.S. Keatley, V.V. Kruglyak, R.J. Hicken, J.R. Childress, and J.A. Katine, *Time-resolved investigation of magnetization dynamics of arrays of non-ellipsoidal nanomagnets with a non-uniform ground state*, Submitted to Physical Review B, under revision.
2. A. Neudert, P.S. Keatley, V.V. Kruglyak, J. McCord, R.J. Hicken, *Selective excitation and imaging of precessional modes in soft-magnetic squares*, Submitted to the proceedings of the IEEE Intermag Conference, Madrid 2008, for publication in the IEEE Transaction on Magnetics, accepted for publication.
3. V.V. Kruglyak, P.S. Keatley, R.J. Hicken, J.R. Childress, and J.A. Katine, *Time-resolved investigation of magnetization dynamics of arrays of non-ellipsoidal nanomagnets with a non-uniform ground state*, Submitted as a chapter in "Spin Wave Confinement" edited by S.O. Demokritov, in press.
4. V.V. Kruglyak, P.S. Keatley, A. Neudert, M. Delchini, R.J. Hicken, J.R. Childress, and J.A. Katine, *Imaging small-amplitude magnetization dynamics in a longitudinally magnetized microwire*, Physical Review B, **77**, 172407 (2008).
5. N.D. Telling, P.S. Keatley, L.R. Shelford, E. Arenholz, G. van der Laan, R.J. Hicken, Y. Sakuraba, S. Tsunegi, M. Oogane, Y. Ando, K. Takanashi, and T. Miyazaki, *Temperature dependence of the interface moments in Co_2MnSi thin films*, Applied Physics Letters, **92**, 192503 (2008).
6. Y. Sakuraba, M. Hattori, M. Oogane, H. Kubota, Y. Ando, A. Sakuma, N.D. Telling, P. Keatley, G. van der Laan, E. Arenholz, R.J. Hicken, and T. Miyazaki, *Extremely large spin-polarization in Co_2MnSi based magnetic tunnel junction*, Journal of the Magnetics Society of Japan, **31**, 338 (2007).

7. V.V Kruglyak, P.S. Keatley, R.J. Hicken, J.R. Childress, and J.A. Katine, *Dynamic configurational anisotropy in nanomagnets*, Physical Review B, **75**, 024407 (2007).
8. S.M. Weekes, F.Y. Ogrin, W.A. Murray, and P.S. Keatley, *Macroscopic arrays of magnetic nanostructures from self-assembled nanosphere templates*, Langmuir, **23**, 1057 (2007).
9. N.D. Telling, P.S. Keatley, G. van der Laan, R.J. Hicken, E. Arenholz, Y. Sakuraba, M. Oogane, Y. Ando, T. Miyazaki, *Interfacial structure and half-metallic ferromagnetism in Co₂MnSi-based magnetic tunnel junctions*, Physical Review B, **74**, 224439 (2006).
10. P.S. Keatley, V.V Kruglyak, R.J. Hicken, J.R. Childress, and J.A. Katine, *Acquisition of vector hysteresis loops from micro-arrays of nano-magnets*, Journal of Magnetism and Magnetic Materials, **306**, 298 (2006).
11. S.M. Weekes, F.Y. Ogrin, and P.S. Keatley, *Configurational anisotropy in hexagonal arrays of submicron Co elements*, Journal of Applied Physics, **99**, 08B102 (2006).
12. V.V Kruglyak, P.S. Keatley, R.J. Hicken, J.R. Childress, and J.A. Katine, *Time resolved studies of edge modes in magnetic nanoelements (invited)*, Journal of Applied Physics, **99**, 08F306 (2006).
13. P.S. Keatley, V.V. Kruglyak, A. Barman, S. Ladak, R.J. Hicken, J. Scott, M. Rahman, *Use of microscale coplanar striplines with indium tin oxide windows in optical ferromagnetic resonance measurements*, Journal of Applied Physics, **97**, 10R304 (2005).

List of Figures

Figure	Description	Page
2.3.1	The precession of a vector about an equilibrium direction is shown.	36
2.4.1	The vector model of orbital angular momentum for a d electron is shown.	38
2.4.2	The Zeeman splitting of a twofold degenerate energy level is shown.	39
2.5.1	The saturation effect in a large magnetic field and at low temperature is shown for the paramagnetic ion Fe^{3+} .	43
2.6.1	The graphical method used to determine the spontaneous magnetisation of a ferromagnetic material is shown.	46
2.6.2	The spontaneous magnetisation as a function of temperature is shown.	47
2.7.1	The variation of the exchange integral as a function of inter-atomic separation is shown for the H_2 molecule.	53
2.8.1	The density of states of the $4s$ and $3d$ bands of a ferromagnetic material is shown for temperatures above and below the Curie temperature.	56
2.9.1	The misalignment of two neighbouring atomic spins is shown.	59
2.9.2	The uniform magnetisation and demagnetising field of an ellipsoidal particle with a single magnetic domain is shown.	63
2.10.1	A typical magnetisation curve and hysteresis loop are shown for a ferromagnetic material. Hypothetical domain configurations are shown for a demagnetised single crystal and polycrystalline sample.	67

Figure	Description	Page
2.10.2	A Bloch wall between two neighbouring ferromagnetic domains of a thin film is shown.	68
2.10.3	The origin of ferromagnetic domains is shown.	69
2.10.4	Hypothetical magnetisation processes are shown.	70
2.10.5	Non-uniform, single domain magnetisation configurations (X-, leaf-, S-, and C-states) are shown for four non-ellipsoidal samples.	71
2.11.1	A single domain ellipsoid with uniform magnetisation and uniaxial shape anisotropy is shown.	72
2.11.2	Hysteresis loops derived using the Stoner-Wohlfarth model are shown.	75
2.11.3	The change in the free energy when a magnetic field is applied is shown.	76
2.13.1	The precession of the magnetisation about the effective magnetic field is shown.	78
2.15.1	A spin wave on a line of spins is shown as the successive advance in phase of the precessional motion of each spin along the line.	82
2.15.2	The Damon-Eshbach magnetostatic mode spectrum for a ferromagnetic slab is shown.	83
2.17.1	Brillouin Light Scattering spectra obtained from transversely, and longitudinally magnetised microscale stripes are shown.	86
2.17.2	Mode profiles and corresponding frequencies of a transversely magnetised microscale stripe are shown.	87

Figure	Description	Page
2.17.3	The experimental spectra obtained from an array of square nanomagnets of different size are shown. For corresponding simulated modes, the spatial distribution of the mode amplitude is shown.	88
3.3.1	The definition of linearly p- and s-polarised light is shown in addition to the Kerr rotation and ellipticity.	96
3.3.2	The geometry used in the calculation of the optical reflection coefficients at a vacuum-magnetic material interface is shown.	97
3.4.1	The polar, longitudinal, and transverse magneto-optical Kerr effect (MOKE) geometries are shown.	99
3.4.2	The calculated Kerr rotation and ellipticity angles for Fe at 800 nm for the polar and longitudinal MOKE geometry is shown.	100
3.4.3	The measured polar Kerr rotation for Ni and Fe is shown as a function of wavelength.	101
3.5.1	The geometry of the scanning Kerr microscope and the set-up of the photodiode bridge polarimeter (bridge detector) is shown.	103
3.5.2	The geometry of the probe laser beam focused upon the sample is shown.	104
3.5.3	The geometry of the Glan-Thompson polarising beam-splitter within the balanced-photodiode bridge detector is shown.	106
3.5.4	Ray tracings are shown for four rays of the probe beam that are sensitive to the out-of-plane component of the sample magnetisation.	107
3.6.1	The cavity layout of the Tsunami femtosecond laser is shown.	109
3.6.2	The experimental set-up of the time-resolved scanning Kerr microscope (TRSKM) is shown.	110

Figure	Description	Page
3.6.3	Fast photodiode signals of the Tsunami pulsed laser output are shown.	112
3.6.4	A typical time-resolved signal, obtained from a 10 μm square element of CoFe/NiFe(13.6 nm), is shown.	113
3.6.5	A typical pulsed magnetic field device is shown.	116
3.6.6	The spatial profile of the pulsed magnetic field is shown.	117
3.6.7	The profile of the current pulse within the pulsed field device is shown.	119
4.2.1	The geometry of the scanning Kerr microscope and the set-up of the quadrant-photodiode polarizing bridge detector (vector bridge) is shown.	129
4.2.2	The geometry of the laser beam focused upon the sample is shown.	131
4.2.3	Ray tracings are shown for two rays from opposite halves of the probe beam that are sensitive to the in-plane component of magnetisation that lies parallel to the applied field.	132
4.2.4	Ray tracings are shown for two rays from opposite halves of the probe beam that are sensitive to the in-plane component of magnetisation that lies perpendicular to the applied field.	133
4.2.5	Scanning electron microscopy (SEM) images of arrays of square elements of length(separation) 637(25), 428(17), 236(77), 124(30), 70(37), 637(236), and 637(688) nm are shown in (a) to (g) respectively. SEM images with higher magnification are shown for the 236, 124, and 70 nm elements in (h) to (j) respectively.	138
4.3.1	Outputs of the vector bridge detector, used to detect the in-plane components of the magnetisation vector, are shown as a function of polariser angle.	140

Figure	Description	Page
4.3.2	Hard axis vector hysteresis loops, obtained from a continuous film of CoFe/NiFe(13.6 nm), are shown.	141
4.3.3	Easy and hard axis hysteresis loops, obtained from a 10 μm square element of CoFe/NiFe(13.6 nm), are shown.	142
4.3.4	Easy and hard axis hysteresis loops obtained from individual microscale elements and arrays of nanomagnets patterned from a CoFe/NiFe(13.6 nm) film are shown.	143
4.3.5	The evolution of the coercive field is shown as the element size is reduced.	144
4.3.6	Simulated hysteresis loops and magnetisation configurations for a single 236 nm element for two directions of the magnetic field, parallel and perpendicular to the uniaxial anisotropy easy axis direction.	146
5.2.1	An optical micrograph shows the indium tin oxide (ITO) window of a hybrid Au/ITO coplanar stripline (CPS) track of a pulsed magnetic field device.	151
5.2.2	The complicated temporal profile of the current pulse in the CPS device is shown.	152
5.3.1	Typical time-resolved Kerr signals, measured by probing a continuous film of permalloy through the ITO window, are shown.	153
5.3.2	Dependence of frequency upon the bias field is shown for time-resolved signals obtained by probing the permalloy film through the ITO window, and between the ITO sections of the CPS.	154
5.3.3	The variation in phase of time-resolved signals measured at various positions across the CPS track is shown with corresponding simulations.	155

Figure	Description	Page
5.3.4	The calculated spatial profile across the CPS is shown for the in-plane and out-of-plane components of the pulsed magnetic field.	157
6.2.1	An optical micrograph of arrays of CoFe/NiFe(13.6 nm) nanomagnets between the tracks of a CPS is shown. Inset is an SEM image of an array of square elements of length(separation) 234(77) nm and a corresponding 3×3 model array used in micromagnetic simulations. The calculated spatial profile of the pulsed magnetic field across the CPS is shown.	162
6.2.2	The dependence of the uniform mode frequency on the bias field value and orientation is shown for a 10 μm square element of CoFe/NiFe(13.6 nm).	163
6.3.1	The simulated static magnetisation states of 3×3 model arrays of 236 nm square elements.	166
6.3.2	The experimental fast Fourier transform (FFT) spectra of time-resolved scans obtained from 236 nm square elements are compared with FFT spectra obtained from different micromagnetic models.	168
6.4.1	A typical raw time-resolved signal, the slowly varying background, and the signal with the background subtracted are shown, in addition to the corresponding FFT spectra, for the array of 236 nm elements at a bias field of 270 Oe.	169
6.4.2	The dependence of the mode frequency upon the element size is shown for bias field values of 1 kOe and 150 Oe. For each element size the simulated spatial distribution of the FFT amplitude of the excited modes is shown.	171
6.4.3	The simulated static magnetisation states within the centre element of 3×3 model arrays are shown.	174

Figure	Description	Page
6.4.4	The dependence of the mode spectra and the spatial character of the different modes upon the bias field is shown for the 637 nm element.	176
6.4.5	The dependence of the mode spectra and the spatial character of the different modes upon the bias field is shown for the 428 nm element.	177
6.4.6	The dependence of the mode spectra and the spatial character of the different modes upon the bias field is shown for the 236 nm element.	179
6.4.7	The dependence of the mode spectra and the spatial character of the different modes upon the bias field is shown for the 124 nm element.	180
6.4.8	The dependence of the mode spectra and the spatial character of the different modes upon the bias field is shown for the 70 nm element.	181
6.4.9	The dependence of the simulated mode spectra and the spatial character of the different modes upon the static magnetisation state of the 3×3 array is shown for the 236 nm element.	183
6.4.10	The simulated total effective field within the centre element of the 3×3 model arrays are shown.	185
6.4.11	Cross-sections of the simulated total effective field within the centre element of the 3×3 model arrays are shown for a bias field of 1 kOe.	186
6.4.12	Cross-sections are shown of the simulated total effective field and mode FFT magnitude within the centre element of the 3×3 model array of 637 nm elements for four values of the bias field.	188

Figure	Description	Page
6.4.13	Cross-sections are shown of the simulated total effective field and mode FFT magnitude within the centre element of the 3×3 model array of 236 nm elements for four values of the bias field.	189
6.4.14	Cross-sections are shown of the simulated total effective field and mode FFT magnitude within the centre element of the 3×3 model array of 70 nm elements for four values of the bias field.	191
6.5.1	Simulated images of the FFT magnitude and phase of the mode spatial character are shown for two modes with frequencies of 6.75 and 7.0 GHz excited in the centre element of a 3×3 array of 236 nm elements at a bias field of 270 Oe. The FFT magnitude is also shown for all elements in the 3×3 array, revealing collective mode excitations.	193
7.2.1	The dependence of the uniform mode frequency on the bias field value and orientation is shown for a 10 μm square element of CoFe/NiFe(2.5 nm).	199
7.3.1	Time-resolved signals and their FFT spectra obtained for different values of the bias magnetic field are shown for the field applied parallel to the edge and the diagonal of 220 nm square elements.	201
7.3.2	Time-resolved signals and their FFT spectra obtained for different orientations of the bias magnetic field are shown for the field value of 589 Oe.	202
7.3.3	Focused, vector hysteresis loops are shown for the case when the magnetic field was applied parallel to the edges of the element and along the element diagonals.	203

Figure	Description	Page
7.3.4	Simulated FFT mode spectra for the centre element in a 3×3 array and for an isolated element in response to a pulsed magnetic field are shown for four different orientations of a bias field of 589 Oe. The spatial character of the excited modes within an isolated element subject to a harmonic magnetic field of the same frequency is shown.	204
7.3.5	The dependence of the calculated mode frequencies and the total effective field averaged over different regions of the sample upon the orientation of the bias magnetic field is shown.	205
8.3.1	A schematic of the new set-up of the TRSKM and microwave probe station used in pulsed magnetic field experiments is shown.	211
8.3.2	Oscilloscope traces of the reflectivity signal are shown as the focused laser spot was placed at different positions relative to the edge of a 6 μm square element. The variation in the reflectivity signal allows the amplitude of the mechanical vibration of the probe station to be estimated.	213
8.3.3	Oscilloscope traces of the capacitive position sensor outputs of the piezoelectric stage are shown in response to an oscillatory input signal.	214
8.3.4	The non-magnetic contrast measured using the in-plane channels of the vector bridge detector as a result of scanning the microscope objective lens is shown.	216
8.3.5	A schematic of the CPS used on the probe station and calculated profile of the in-plane and out-of-plane components of the pulsed magnetic field are shown.	218
8.3.6	Traces of the current pulse profile are shown before and after the pulse is transmitted through the CPS.	219

Figure	Description	Page
8.3.7	Time-resolved scans obtained using the probe station and the previous experimental set-up are compared.	220
8.4.1	The reflectivity signal and the Kerr rotation are shown as a function of ZnS anti-reflective coating (ARC) thickness.	222
8.4.2	Vector hysteresis loops and time-resolved scans acquired from a 6 μm diameter disc patterned from a PtMn(25 nm)/CoFe(8 nm)/Al ₂ O ₃ (0.7 nm)/[CoFe/NiFe](2.5 nm) tunnel-valve stack with and without a ZnS(33 nm) ARC deposited on top of the sample are compared.	224
8.5.1	The new vector bridge longitudinal Kerr signal output, used to detect the in-plane component of the magnetisation vector, is shown as a function of polariser angle.	226
8.5.2	Vector hysteresis loops acquired using the new vector bridge are shown for a CoFe/NiFe(13.6 nm) 10 μm square element and arrays of square nanomagnets of size 234, 124, and 70 nm.	227
8.5.3	A time-resolved scan acquired using the probe station and the corresponding Fourier spectrum is shown for a 40 μm square of (Fe ₉₀ Co ₁₀) ₇₈ B ₁₂ Si ₁₀ (160 nm).	228
8.5.4	A schematic of the set-up of the TRSKM and microwave probe station used in harmonic magnetic field experiments is shown.	229
8.5.5	Vector- and time-resolved scans and images of the dynamic magnetisation are shown for two modes with frequency 8.0 GHz and 9.2 GHz that are excited in the 40 μm square of (Fe ₉₀ Co ₁₀) ₇₈ B ₁₂ Si ₁₀ (160 nm).	230
A2.1	Raw time-resolved scans obtained from an array 637 nm elements of CoFe/NiFe(13.6 nm) are shown for different bias field values.	238

Figure	Description	Page
A2.2	Raw time-resolved scans obtained from an array 428 nm elements of CoFe/NiFe(13.6 nm) are shown for different bias field values.	238
A2.3	Raw time-resolved scans obtained from an array 236 nm elements of CoFe/NiFe(13.6 nm) are shown for different bias field values.	239
A2.4	Raw time-resolved scans obtained from an array 124 nm elements of CoFe/NiFe(13.6 nm) are shown for different bias field values.	239
A2.5	Raw time-resolved scans obtained from an array 70 nm elements of CoFe/NiFe(13.6 nm) are shown for different bias field values.	239
A3.1	Detailed drawings of the probe station assembly are shown.	240
A3.2	Detailed drawings of the probe station assembly cross section are shown.	241
A3.3	Detailed drawings of the piezoelectric microscope mount are shown.	241
A3.4	Detailed drawings of the microwave probes are shown.	242
A4.4-9	A series of photographs show the procedure for tuning the capacitive position sensor servomechanism loop gain for the piezoelectric stage.	243
A5.1	The electronic circuit for the Mk II vector bridge is shown.	244
A5.2	The Mk II vector bridge output T2+T1 and P2-P1, used respectively to detect the second in-plane component and the out-of plane component of the magnetisation vector, is shown as a function of polariser angle.	245

List of Tables

Table	Description	Page
2.11.1	Solutions of the minimised free energy equations, derived using the Stoner-Wohlfarth model, are given.	73
2.11.2	The components of the magnetisation parallel to the applied field, derived using the Stoner-Wohlfarth model, are given.	74
3.7.1	Cables that may emit electromagnetic radiation at the reference frequency of the phase sensitive detection scheme for time-resolved measurements are listed.	125
4.2.1	The pad designation of the quadrant photodiode sum and difference amplifier outputs is given.	130
4.2.2	The table lists all ten outputs of the vector bridge detector and their corresponding experimental function.	136

Declaration

The work presented in this thesis is the result of the joint effort of many people. The contribution to this work by my colleagues is outlined below and will be acknowledged more specifically throughout the main text of this thesis. Particular contributions to this work by my PhD supervisor, Prof Rob Hicken, are difficult to describe as they permeate the whole of this thesis.

Chapter 1 *Introduction*

The introduction to the work presented in this thesis and the description of the motivation for conducting research in this area of physics is my own work. Details published by other authors that have been used in the discussions in Chapter 1 have been acknowledged.

Chapter 2 *Background principles of magnetism*

The background principles of magnetism relevant to this thesis have been compiled by myself in Chapter 2. The principles discussed in Chapter 2 are not the result of my own work. Throughout Chapter 2 the reference material used for each discussion has been acknowledged.

Chapter 3 *Experimental techniques*

The background principles of magneto-optics relevant to this thesis have been compiled by myself in Sections 3.2 to 3.4 of Chapter 3. However, the principles discussed in these sections are not the result of my own work. Throughout these sections the reference material used for each discussion has been acknowledged. In Sections 3.5 to 3.7 the description of the experimental techniques represents my own work. The basis for time-resolved experiments in Exeter had been set up by Prof Rob Hicken, Dr Jing Wu, Dr Ralph Wilks, Dr Anjan Barman, and Dr Volodymyr Kruglyak before I started my PhD project. The time-resolved scanning Kerr microscope (TRSKM) was set up by Dr Barman. The experiments presented in Chapter 5 were performed by myself using the TRSKM set up by Dr Barman. The experiments presented in Chapters 4, 6, 7 were performed using the TRSKM set up by myself with advice from Dr Kruglyak and Prof Hicken. Data acquisition software was written by Prof Hicken, Dr Barman, Dr Wilks and myself.

Chapter 4 Acquisition of vector hysteresis loops from microarrays of nanomagnets

The microscale elements and microarrays of nanomagnets were fabricated by Dr Jeffrey Childress and Dr Jordan Katine at Hitachi Global Storage Technologies San Jose Research Center, California. The scanning Kerr microscope was set up by myself. The vector bridge detector was designed originally by Dr Anjan Barman. The mechanics were constructed by Mr Kevyn White and the electronics were built by Dr Barman. The original vector bridge was unsuccessful in the achieving vector sensitivity. Realignment of the quadrant photodiodes and modification of the detector electronics was carried out by myself in order to achieve vector sensitivity. The characterisation of the vector sensitivity, and the acquisition of hysteresis loops from individual microscale elements and microarrays of nanomagnets was carried out by myself.

Chapter 5 Use of microscale coplanar stripline with indium tin oxide windows in optical ferromagnetic resonance measurements

The hybrid Au/indium tin oxide coplanar stripline was fabricated by Dr Jamie Scott and Dr Mahfuzur Rahman at the University of Glasgow. The permalloy film was fabricated by Dr Sam Ladak at the University of Exeter. The TRSKM was set up by Dr Anjan Barman. The sample was prepared by Dr Barman and myself, while measurements and data analysis were carried out by myself.

Chapter 6 Time-resolved investigation of magnetisation dynamics of arrays of non-ellipsoidal nanomagnets with a non-uniform ground state

The microscale elements and microarrays of nanomagnets were fabricated by Dr Jeffrey Childress and Dr Jordan Katine at Hitachi Global Storage Technologies San Jose Research Center, California. The TRSKM was set-up by myself. The measurements were carried out primarily by myself with additional help from Dr Volodymyr Kruglyak. The data analysis and micromagnetic simulations were carried out by myself, except for the macrospin fitting, which was carried out by Dr Kruglyak. The parameter files used in the micromagnetic simulations were based on those originally written by Dr Kruglyak. The analysis software for micromagnetic simulations was written by Dr Evgeny Galaktionov.

Chapter 7 *Dynamic configurational anisotropy in nanomagnets*

The microscale elements and microarrays of nanomagnets were fabricated by Dr Jeffrey Childress and Dr Jordan Katine at Hitachi Global Storage Technologies San Jose Research Center, California. The TRSKM was set-up by myself. The time-resolved measurements were carried out by myself and Dr Volodymyr Kruglyak. The vector hysteresis loop measurements were carried out by myself. The data analysis and micromagnetic simulations were carried out by Dr Kruglyak.

Chapter 8 *Recent developments for future work*

The microwave probe station was designed by myself, Prof Rob Hicken, and Mr Russell Edge. The electromagnet, sample stage, and piezoelectric stage bracket for the microscope column were built by Mr Edge. Additional supports for vibration control of the sample stage were built by Mr Kevyn White. All measurements for the characterisation of the mechanical vibration were carried out by myself. The tuning of the piezoelectric stage servomechanism loop gain was carried out by myself. The new coplanar stripline was fabricated by Dr Volodymyr Kruglyak. The current pulse profiles were measured by Dr Kruglyak and Dr Andreas Neudert. Antireflective coatings (ARC) were deposited by Mr David Jarvis. Characterisation of the enhancement of the magneto-optical effect for different ARC thicknesses was carried out by myself. The microscale elements (6 or 10 μm) and microarrays of nanomagnets were fabricated by Dr Jeffrey Childress and Dr Jordan Katine at Hitachi Global Storage Technologies San Jose Research Center, California. The 40 μm sized element sample was fabricated by Dr Michael Frommberger at the Center of Advanced European Studies and Research, Smart Materials Group, Germany. The new vector bridge detector was designed by myself. The mechanics were constructed by Mr White, while the electronics were built by myself. Advice on the construction of the electronics was given by Dr Charles Williams, Mr Tom Addison, and Mr Chris Forrest. Vector hysteresis loops were acquired by Mr Marco Delchini under my supervision during his summer research project in Exeter. Vector- and time-resolved measurement of images of the dynamic magnetisation of the 40 μm element were carried out by Dr Neudert. Testing of the synchronisation of the electronic pulse generators and microwave synthesisers with the pulsed laser was carried out by Dr Neudert and Dr Kruglyak.